Construction of Acid–Base Synergetic Sites on Mg-bearing BEA Zeolites Triggers the Unexpected Low-Temperature Alkylation of Phenol

Jingyan Xie,[a] Wenxia Zhuang,[a] Wei Zhang,[a] Ning Yan,[b] Yu Zhou,*[a] and Jun Wang*[a]

Novel Mg-bearing BEA zeolites are synthesized to simultaneously endow significantly enhanced basicity without compromising acidity over the zeolite framework. Serving as efficient solid acid–base bifunctional catalysts, they achieve the liquid-phase selective methylation of phenol with methanol to produce *o*- and *p*-cresol ($o/p=2$) under mild conditions. The method is readily extendable to the alkylation of phenols with various alcohols. Stereo- and regioselectivity (>95% for *p*-product) was attained on the alkylation of phenol with bulky *tert*-butyl alcohol, rendering the first acid–base cooperative shape-selective catalysis relying on the basicity of zeolites. A preliminary mechanistic analysis reveals that the remarkable activity and shape-selectivity come from the superior special acidic–basic synergetic catalytic sites on the uniform microporous channels of the BEA zeolite.

Introduction

Alkylation of aromatic hydrocarbons is a large industrial process with the products covering numerous petrochemicals and fine chemicals.[1–3] The processes are usually carried out over acid catalysts.[4–6] For example, acid-catalyzed alkylation of benzene with ethylene or propylene is used to produce two important bulk chemicals of ethylbenzene and isopropylbenzene.[7,8] Compared with liquid acids, solid acids are preferred owing to their various advantages, but the majority of them take place at high temperature and in the gas phase.[9–11] Nowadays, energy saving and environmental friendliness are the two major elements involved in the development of sustainable chemical processes,[12–17] preferring low-temperature liquid-phase alkylation processes.[18,19] However, solid acids usually suffer from low activity in such cases, thus it is greatly attractive and a challenge to develop new efficient solid acid catalysts towards the target low-temperature liquid-phase alkylation process.

Among the various alkylation reactions, methylation of phenol with methanol is one industrially available pathway to produce cresols, important intermediates for manufacturing functional polymers, antioxidants, pharmaceuticals, and agrochemicals. Various catalysts have been developed, such as metal oxides,[20–22] zeolites,[23–25] sulfates,[26] mixed metal oxides,[27–30] and hydrotalcites.[31] MCM-22 with different Si/Al has only approximately 20% selectivity for the C-alkylation of phenol at low pressure.[32] H-Beta zeolites with different crystal sizes have been investigated for their effect on catalytic performance for phenol methylation. Deactivation is triggered by phenol and polyalkylated phenol derivatives with extending reaction time.[23] Zeolite Zn^{2+}/NaY generates strong Lewis acid sites that efficiently activate the phenol methylation reaction. However, the zeolite activity decays increasingly with the concomitant increase of sample acidity.[33] Zeolites as catalysts promote the O-alkylation at medium temperatures. Low-temperature liquid-phase reactions can relieve deactivation resulting from cooking. Only one report of the liquid-phase alkylation of phenol with methanol has been reported, in which zeolite catalysts HZSM-5 and HMCM-22 were used, giving a maximum yield of approximately only 2%.[34]

Zeolites are well-known microporous molecular sieves that can be used as environmentally benign catalytic materials with large-scale applications in industry, particularly in refinery/petrochemical processes and the production of fine chemicals.[35–38] They are usually used as solid acids because the framework tetrahedral aluminum species provide internal Lewis acid sites and the protons present as the counter cations show Brønsted acidity.[36] However, their acid strength is far from that of liquid acids (such as H_2SO_4, HCl, HF), giving rise to inferior activity in low-temperature reactions, which is so far one unresolved issue. Many approaches have been proposed to improve the performance of solid acids under mild conditions. One efficient way is the fabrication of acid–base bifunctional sites that can reach high activity and selectivity, reduce the operating temperature and side reactions.[39–41] Nevertheless, the approach is rarely successful for zeolites owing to the

[a] J. Xie, W. Zhuang, W. Zhang, Dr. Y. Zhou, Prof. Dr. J. Wang
State Key Laboratory of Materials-Oriented Chemical Engineering, College of Chemical Engineering
Nanjing Tech University (former Nanjing University of Technology)
Nanjing, Jiangsu 210009 (P.R. China)
E-mail: njutzhouyu@njtech.edu.cn
junwang@njtech.edu.cn

[b] Prof. Dr. N. Yan
Department of Chemical and Biomolecular Engineering
National University of Singapore, 4 Engineering Drive 4
Singapore 117585 (Singapore)

Supporting information for this article can be found under: http://dx.doi.org/10.1002/cctc.201601127.

lack of robust basic sites, let alone for the construction of efficient acid–base synergetic active sites in the zeolite channels.

In this work, superior framework acidity and basicity are simultaneously constructed by incorporating Mg ions into the framework of BEA zeolites in a hydrothermal synthesis pathway involving a special acid co-hydrolysis route. Modification through ion-exchange with transitional metal ions is performed to improve their basicity. Catalyzed by these Mg-bearing zeolites, the low-temperature liquid-phase methylation of phenol with methanol to produce *o*-/*p*-cresols is achieved with high cresols yield and stable reusability. The influence of reaction conditions such as temperature, time, and molar ratio of substrates are systematically investigated. Various control catalysts are tested in parallel to gain insight into the reaction. In situ FTIR spectra of adsorbed substrates are performed to further understand the mechanism. Alkylation of phenol with various alcohols is attained with the same method. With the bulky substrate *tert*-butyl alcohol, high stereo-/regioselectivity (>95% for the *para* product) is achieved thanks to the special nano-confinement in the zeolite channels.

Results and Discussion

Mg-bearing BEA zeolites were synthesized in a one-pot hydrothermal process involving an acidic co-hydrolysis route (Scheme S1 in the Supporting Information). We have revealed that the acidic co-hydrolysis route favors the incorporation of heteroatoms in the zeolite synthesis.[42,43] Controlling the pH value in the initial co-hydrolysis/condensation of tetraethylorthosilicate (TEOS) and magnesium nitrate gives the highly crystallized zeolites with BEA phase, as confirmed by the XRD patterns (Figure 1 A and Figure S1 in the Supporting Information). By contrast, no zeolite phase is detected from the direct hydrolysis of the magnesium salt and TEOS under basic conditions (Figure S1 in the Supporting Information). For the hydrolysis and condensation of silica precursors, acidic conditions offer a lower rate than basic ones; when together with metal ions, the acidic conditions (rather than basic ones) allows more isolated metal ions to be created, which readily form bond linkages between the metal ions and silanol groups.[42,43] In this work, the acid co-hydrolysis route is thus more likely to generate the desirable Si-O-Mg-O-Si-O-Al units, that is, the primary building blocks for further growth of the Mg-containing zeolite crystals, which may account for the indispensable role of the acidic conditions in this synthesis. The directly synthesized Mg-containing samples are named Mgβ(*n*) (*n*=100, 55, or 33, denoting the Si/Mg molar ratio in the gel). Chemical composition analyses by inductively coupled plasma (ICP; Table 1) demonstrate the incorporation of Mg species in Mgβ(*n*) with the Si/Mg molar ratios of 151, 109, and 115 for *n*=100, 50, and 33. All the samples have similar SiO_2/Al_2O_3 molar ratios of approximately 31. Characterizations by SEM, TEM, thermogravimetric analysis (TGA), nitrogen sorption measurements, and ^{29}Si and ^{27}Al NMR spectroscopic analyses confirm the crystal structure has the morphology of ellipsoid-globose of 1–2 μm, has a homo-dispersion of Mg ions, high thermal stability, and abundant open microporosity (Table 1, Figure 1, and

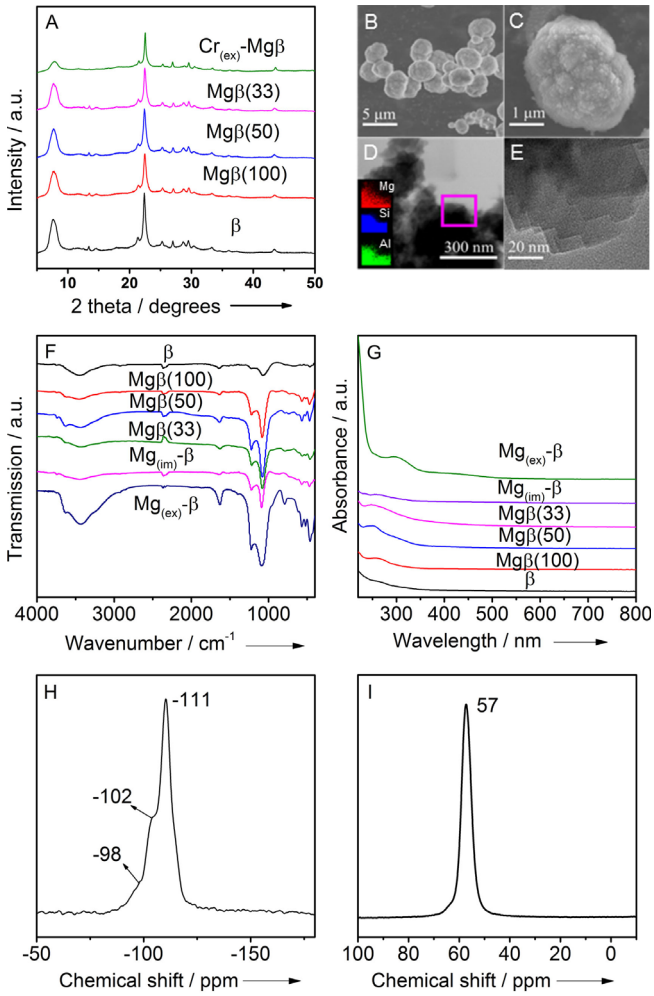

Figure 1. A) XRD patterns of Mg-bearing zeolites and β. B), C) SEM images of Mgβ(50). D), E) TEM images with Si, Al, and Mg elemental mapping images of Mgβ(50). F) IR and G) UV/Vis spectra of different samples. H) ^{29}Si and I) ^{27}Al MAS NMR spectra of Mgβ(50).

Table 1. Textural properties of various BEA zeolites and contrast samples.

Sample	Si/Me[a] [mol mol^{-1}]	SiO_2/Al_2O_3[b]	Surface area [m^2 g^{-1}]	Pore volume [cm^3 g^{-1}]
Mgβ(100)	151	32.75	519	0.27
Mgβ(50)	109	30.09	598	0.33
Mgβ(33)	115	31.24	566	0.32
$Cr_{(ex)}$-Mgβ	95[c]/131[d]	31	548	0.43
β	–	36.57	622	0.25

[a] Molar ratio of Si to Me for the final solid products. [b] Molar ratio of SiO_2 to Al_2O_3 for the final solid products. [c] Molar ratio of Si to Cr for the final solid. [d] Molar ratio of Si to Mg for the final solid. All the molar ratios are determined by ICP.

Figures S2–S4 and Table S1 in the Supporting Information). Further, the unit-cell volume of Mgβ(*n*) is apparently enlarged (Table S2 in the Supporting Information); also, the samples exhibit an IR band shift to approximately 1072 cm^{-1} for the tetrahedral TO_4 units and new UV/Vis absorbance at approximately 245 nm.[44] In contrast, these variations are all absent for the parent β, control samples of $Mg_{(ex)}$-β (Mg ion-exchanged β)

and $Mg_{(im)}$-β (MgO-loaded β by impregnation) (Figure 1 F and G). The observations are similar to previous Mg-containing zeolites,[45] suggesting the formation of framework Mg ions that differ from ion-exchanged and impregnated Mg species.

The X-ray photoelectron spectroscopy (XPS) core-level spectra were collected on the typical sample Mgβ(50) plus the controls of β, $Mg_{(ex)}$-β, and $Mg_{(im)}$-β. In the O 1s spectra, peaks appear at 532.85, 533.5, 534.5, and 536 eV, respectively, for Mgβ(50), $Mg_{(im)}$-β, $Mg_{(ex)}$-β, and β (Figure 2 A). A significant shift

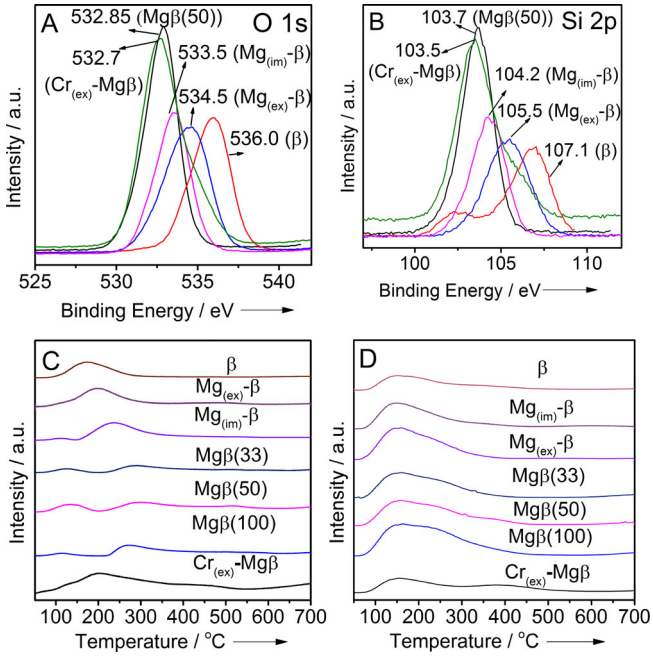

Figure 2. A) O 1s and B) Si 2p XPS spectra for samples. C) CO_2-TPD and D) NH_3-TPD curves for samples.

to lower binding energies is observed for Mgβ(50) in contrast to β, which is attributable to the incorporated Mg ions with weak electronegativity, which increases the electron density of O atoms.[46] The Si 2p peak is centered at around 107.1 eV for β, which shifts to 105.5, 104.2, and 103.7 eV for $Mg_{(ex)}$-β, $Mg_{(im)}$-β, and Mgβ, respectively (Figure 2 B). The observed similar shifts towards lower binding energies of Si 2p can be assigned to the change in the polarizability of oxygen, indicating the formation of a less stoichiometric SiO_2 phase.[47,48] A more significant shift of the O 1s and Si 2p signals occurs for Mgβ(50) than for $Mg_{(im)}$-β and $Mg_{(ex)}$-β, suggesting that in situ incorporated Mg species favors more negative O species, in accordance with our previous observations.[49,50]

The basicity of zeolites is closely related to the negativity of O species and more negative O species usually mean enhanced basicity.[45] In the CO_2 temperature-programmed desorption (TPD) curves, the Mgβ(*n*) samples demonstrate three CO_2 desorption peaks in the ranges of 110–130 °C, 270–300 °C, and 500–520 °C, respectively identified to the weak, medium, and strong basic sites (Figure 2 C).[51] On the contrary, bare β only presents a peak centered at 170 °C, confirming the enhanced basicity of Mgβ(*n*). As for the acidic properties of Mgβ(*n*), NH_3-TPD results (Figure 2 D) reflect that they exhibit similar NH_3-TPD curves as the parent β with only a slight decrease of the shoulder peak at 250 °C, suggesting that the majority of the acidity is preserved after Mg incorporation. All the above phenomena reveal much enhanced basicity with well retained super acidity for the Mgβ(*n*) samples.

A chromium ion-exchanged sample, $Cr_{(ex)}$-Mgβ, was prepared from Mgβ(50). Structural characterizations by XRD, SEM, and nitrogen sorption experiments reveal the preservation of the parent structure (Figure 1 A, Figures S2 and S4 in the Supporting Information, and Table 1). The ICP analysis shows that $Cr_{(ex)}$-Mgβ contains a similar Mg content as Mgβ(50) and has the Si/Cr molar ratio of 95. XPS and TPD results indicate that $Cr_{(ex)}$-Mgβ exhibits additionally enhanced basicity and acidity compared with its parent counterpart Mgβ(50) (Figure 2).

The Mg-bearing BEA zeolites were next used as heterogeneous catalysts in the low-temperature liquid-phase methylation of phenol with methanol. The reaction and even the side reactions do not occur in the absence of catalyst, but Mgβ(*n*) can efficiently catalyze the methylation reaction. Mgβ(50) (Table 2,

Table 2. Liquid-phase methylation of phenol with methanol.[a]

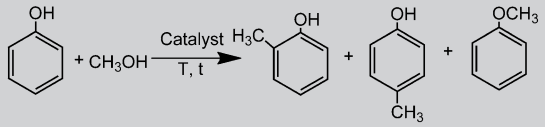

Entry	Catalyst	C_{phenol} [%][b]	Y_{cresol} [%][c]	$Y_{anisole}$ [%][d]	S_{methyl} [%][e]	Acid sites [mmol g^{-1}][f]	Base sites [mmol g^{-1}][g]
1	Mgβ(50)	35.8	15.7[h]	19.1	97.2	1.58	0.93
2	$Cr_{(ex)}$-Mgβ	49.8	30[h]	15.3	91.0	1.15	1.28
3	$Mg_{(ex)}$-β	9.6	2.8[h]	5.7	88.5	1.42	0.60
4	$Mg_{(im)}$-β	0.6	0	0.2	33.3	1.22	0.52
5	β	0.5	0.04	0	8.0	1.21	0.50
6	Hβ	1.4	0.6	0.6	85.7	1.41	0.48
7	γAl_2O_3	4.1	1.1	3	99.9	0.32	0.06
8	MgO	0.8	0	0.5	62.5	0.07	0.21
9	MgO@γAl_2O_3	9.0	0.15	4.6	52.8	0.25	0.51

[a] Reaction conditions: 10 mmol phenol, 35 mmol methanol, 190 °C, 18 h, 0.1 g catalyst. [b] Conversion: [mmol (phenol converted)]/[mmol (phenol initial)] × 100. [c] Yield: [mmol (cresols)]/[mmol(initial phenol)] × 100. [d] Yield: [mmol (anisole)]/[mmol (initial phenol)] × 100. [e] Selectivity of the methylation product: [mmol (cresols + anisole)]/[mmol (initial phenol)] × 100. [f] Total amount of acid sites measured by NH_3-TPD. [g] Total amount of base sites measured by CO_2-TPD. [h] The molar ratio of *o*- to *p*-cresol is 2.

entry 1) gives 15.4 % yield of cresols ($o/p = 2$) at the optimized conditions (Figure 3), which is slightly higher than the Mgβ(33 and 100) samples (Table S3, entries 1–2). Besides the C-methylation products, cresols, there is also the O-methylation product, anisole, another industrially important chemical intermediate. The yield of anisole over Mgβ(50) is 19.1 %. Few coking or other byproducts were detected, with the total selectivity for methylation products being 97.2 %. The catalytic performance of Mgβ(50) under different conditions was explored by varying the temperature, time, and phenol/methanol molar ratio

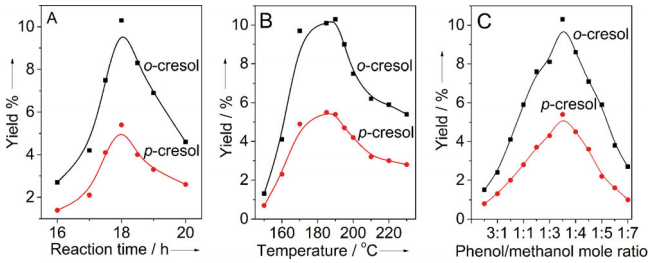

Figure 3. A) Cresol yields as a function of reaction time over Mgβ(50). Reaction conditions: 10 mmol phenol, 35 mmol methanol, 190 °C, 0.1 g catalyst. B) Cresol yields as a function of reaction temperature over Mgβ(50). Reaction conditions: 10 mmol phenol, 35 mmol methanol, 18 h, 0.1 g catalyst. C) Effect of molar ratio of phenol and methanol on yield over Mgβ(50). Reaction conditions: 190 °C, 18 h, 0.1 g catalyst.

(Figure 3). The yield as a function of each parameter presents volcanic-type curves. With longer reaction time (> 18 h) or higher temperature (> 190 °C), the yield declines owing to additional side reactions of the formed cresols.

After reaction, the catalyst can be facilely separated by filtration and reused. The three-run recycling assessment for Mgβ(50) reveals a clear decrease in activity (Figure 4 A). The

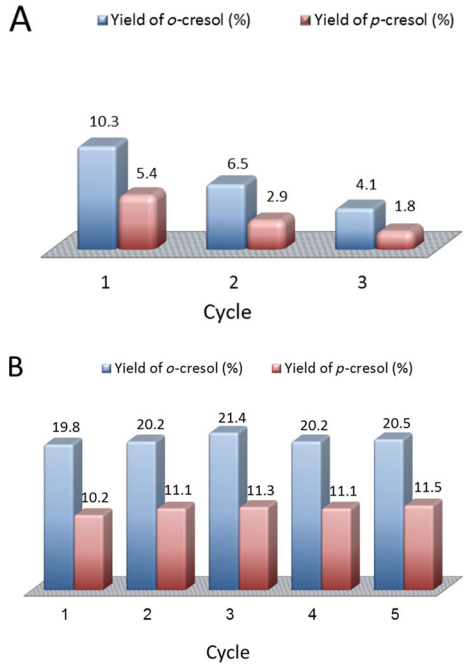

Figure 4. Catalytic reusability of A) Mgβ(50) and B) $Cr_{(ex)}$-Mgβ in the methylation of phenol. Reaction conditions: 10 mmol phenol, 35 mmol methanol, 190 °C, 18 h, 0.1 g catalyst.

reason can be assigned to the decreased surface area, Mg content, and corresponding basicity of the reused sample (Table S1 and Figure S5 A in the Supporting Information). Ion-exchange with metal ions is one facile and widely adopted way to modify zeolites. Various metal ions (Mg, Cs, Cr, Ce, V, Cu, and Nb) were selected as counter cations of Mgβ(50) by referring to their promotion effect for the reaction under gas-phase conditions (Table S3 in the Supporting Information, entries 3–8).[52] $Cr_{(ex)}$-Mgβ (Table 2, entry 2) demonstrates a high yield of 30 % for cresols and 15.3 % for anisole with the methylation selectivity of 91.0 %, whereas the others are inert (< 3 %, Table S3 in the Supporting Information). Moreover, stable activity is observed over $Cr_{(ex)}$-Mgβ in a five-run recycling test (Figure 4 B), thanks to the well preserved structure (Figures S4–S6 and Table S1 in the Supporting Information).

The effect of catalysts was investigated over various solid acid and base catalysts (their structural information is given in Figures S2, S4, S7, and Table S1 in the Supporting Information). As shown in Table 2, $Mg_{(ex)}$-β gives much low activity (entry 3, 2.8 %) whereas $Mg_{(im)}$-β is inactive (entry 4, 0 %). No or trace amounts of cresols were detected over β (entry 5, 0 %), solid acids like Hβ (entry 6, 0.6 %) and γAl_2O_3 (entry 7, 1.1 %), commercial solid base MgO (entry 8, 0 %), or solid acid–base catalyst MgO@γAl_2O_3 (entry 9, 0.15 %); although they were active in the high-temperature gas-phase methylation reaction.[22,23] These observations suggest that neither solid base nor solid acid are effective for the reaction. Instead, methylation requires both acid and base sites. Nonetheless, basicity introduced through impregnation (that is, $Mg_{(im)}$-β and MgO@γAl_2O_3) almost damage the activity, demonstrating that such separated acid and base sites fail to promote the catalysis. Ion-exchange with alkaline or alkaline-earth metal ions favors the increase of zeolite basicity, in which the basic sites are adjacent to the acid ones, forming cooperative acid–base pairs with more negative O than its parent. Thus, catalytic activity, though still low, is observed over $Mg_{(ex)}$-β. Similarly, low activity is detected over other analogues (Table S3 in the Supporting Information, 3.1, 2.2, 1.6, and 1.1 % for Ca, Ba, Sr, and $Cs_{(ex)}$-β). Their low activity is attributable to the weak basicity and decreased acidity (Figure S8 and Table S4 in the Supporting Information). For our newly prepared Mgβ series, incorporation of Mg ions into the framework of the BEA zeolite generates acid–base pairs with not only well-retained original acidity but much more negative O, denoting enhanced basicity, which thus promotes the reaction. Further improved performance of $Cr_{(ex)}$-Mgβ can be assigned to additionally enhanced basicity and acidity. Based on the above comparison, we propose that sufficient activation of the substrates in the low-temperature liquid-phase methylation of phenol requires synergetic interaction of adjacent acid–base pairs with both superior acidity and basicity within the zeolite framework.

Other Mg-bearing zeolites MgS-1, Mg-ZSM-5, and Mg-MOR are totally inactive (0 %) in the reaction (Table S3, entries 7–9 in the Supporting Information), because incorporation of Mg ions improves their basicity but decreases the acidity (Figure S8 and Table S4 in the Supporting Information). These results, on the one hand, support the above supposition that the reaction requires both superior acidity and basicity; on the other hand, it implies the uniqueness of incorporating Mg ions into the BEA framework, which enhances the basicity while simultaneously preserving the initial acidity of the zeolites.

In situ FTIR spectra were performed to provide insight into the above liquid-phase methylation of phenol with methanol (Figure 5). The band assignments are listed in Tables S5–S7 in

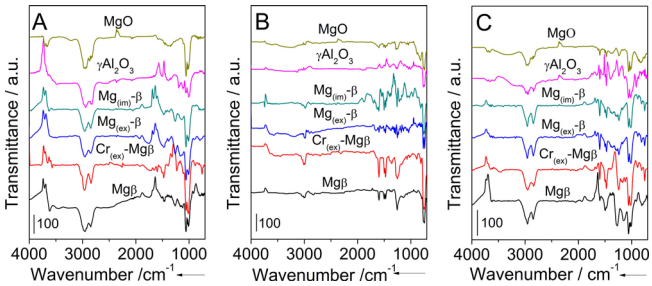

Figure 5. FTIR spectra of A) methanol, B) phenol, and C) mixture of phenol and methanol with the mole ratio of 1:3.5 adsorbed on different samples at 190 °C.

the Supporting Information. Figure 5 A shows the FTIR spectra of adsorbed methanol. The bands of adsorbed methanol on MgO are similar to gas-phase methanol, suggesting weak interactions between adsorbed methanol and MgO under these conditions. γAl_2O_3 also shows weak adsorption but exhibits negative bands at approximately 3750–3650 cm^{-1}, which can be assigned to the consumption of surface Al–OH as a result of the interaction of adsorbed methanol with these hydroxyl groups. Correspondingly, the negative bands around 1400–1600 cm^{-1} also come from the consumption of these hydroxyl groups. Such phenomena indicate that methanol is mainly weakly adsorbed on surface of γAl_2O_3 through the interaction of methanol with the surface hydroxyl group. Mg-bearing zeolites demonstrate strengthened adsorption to methanol with certain variations of the bands differing from the gas phase. Similar negative peaks as γAl_2O_3 are observed for these samples, implying that some methanol is adsorbed through interaction with surface hydroxyl groups. Apparent shifting or splitting is observable for the bands around 1350–1500 cm^{-1}, which are attributable to the C–H stretching vibration and COH deformation vibration.[22,53] The band at approximately 1250 cm^{-1} is attributable to O–H deformation vibration perceived from the zeolite catalyst. These observations reflect the deformation of adsorbed methanol on these zeolites with the elongation of C–O–H, which causes the activation of adsorbed methanol.

The FTIR spectra of adsorbed phenol (Figure 5 B) reveal that strong adsorption of phenol takes place on Mgβ(50) and $Cr_{(ex)}$-Mgβ. Significant variation of the adsorption bands from those of gas-phase phenol is observable. The band assigned to phenolic O–H deformation vibrations splits into two components at approximately 1400 and 1350 cm^{-1}.[53,54] An intense band at 1253 cm^{-1} is attributable to the C–O stretching vibration of adsorbed phenol with strong interaction with the surface acid–base pairs. These phenomena reflect a strong chemical adsorption of phenol on Mgβ(50) and $Cr_{(ex)}$-Mgβ. No bands are observed from 1800 to 2000 cm^{-1}, revealing a parallel adsorption of phenol on these two samples.[53] Weak adsorption of phenol takes place on MgO and γAl_2O_3, and these bands are close to those of gas-phase phenol, reflecting their weak interactions with phenol. Certain chemical adsorptions occur on $Mg_{(im)}$-β and $Mg_{(ex)}$-β. The weak band located at 1250 cm^{-1} reveals a small amount of deformed phenol molecules on the surface. The bands at 2008 and 1857 cm^{-1} for the out-of-plane C–H bending vibration is an indication of the perpendicular orientation of adsorbed phenol on $Mg_{(im)}$-β.[53] In the case of a mixed solution (phenol/methanol = 1:3.5, the same as in the alkylation of phenol with methanol), strong co-adsorption of methanol and phenol is still observable on Mgβ(50) and $Cr_{(ex)}$-Mgβ, whereas weak adsorption occurs on MgO, γAl_2O_3, $Mg_{(im)}$-β, and $Mg_{(ex)}$-β (Figure 5 C). These phenomena suggest that Mgβ(50) and $Cr_{(ex)}$-Mgβ can chemically adsorb the methanol and phenol in the mixed solution to reach sufficient activation.

Basing on the above in situ FTIR results, a possible route for the Mg-bearing BEA zeolites to catalyze the methylation of phenol with methanol is proposed in Scheme 1 A. Methanol and phenol are chemically adsorbed on Mgβ(50) and $Cr_{(ex)}$-Mgβ. Conjunct acid–base pairs within the 12-membered-ring (12-MR) channel provide sufficient driving force for the adsorption through the mode in Scheme 1 A. The positive Al (acid site) and negative O species (basic site) respectively exert strong interactions with the hydroxyls of methanol and phenol, in which phenol is adsorbed in a parallel fashion.[53] Simultaneous activations of the two substrates is attained as a result of such strong adsorption. The carbocation is formed from methanol on the Lewis acid site of Al cations, whereas the electron donor effect of the phenol OH group increases

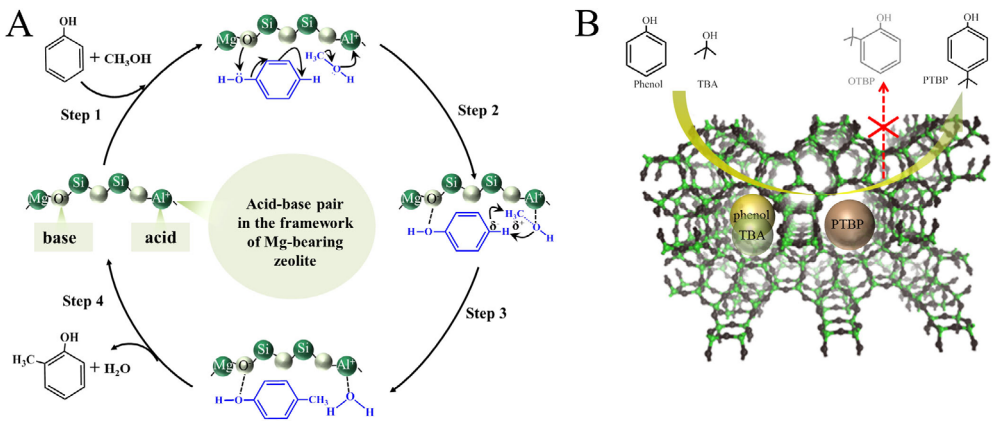

Scheme 1. A) Possible reaction mechanism for the methylation of phenol over Mgβ(50). B) Product selectivity mechanism.

the electronic density of the *o*- and *p*-positions, strengthened by Mg-derived negative O basic site. Then, taking the *p*-position as an example, the carbocation attacks the nearby parallel adsorbed phenol ring and one benzene ring proton is released to the hydroxyl of methanol with the formation of water. Finally, by such electrophilic substitution, *p*-cresol is produced. Each attacking probability at the *o*- or *p*-position is equal, thus causing the 2:1 molar ratio of *o*- and *p*-cresol. In addition, the carbocation can also attack the O-position to form anisole. No cresol forms by using anisole to replace phenol, thus excluding the possible route from the rearrangement of anisole and further supporting the above mechanism. By contrast, only weak adsorption takes place on γAl_2O_3 and MgO, suggesting that solid acid or base alone cannot provide enough host–guest interactions to activate the reactants, especially in the coexistence of phenol and methanol as a result of competing adsorption. $Mg_{(im)}$-β and $Mg_{(ex)}$-β can adsorb methanol but weakly capture phenol, thus also failing to efficiently activate them. Therefore, the reaction cannot efficiently proceed over these catalysts.

The reaction scope was extended by evaluating other alcohols including ethanol, isopropanol, and *tert*-butyl alcohol (Table 3). All of them show good activities with the yields over

Table 3. Liquid-phase alkylation of phenol with different alcohols.[a]

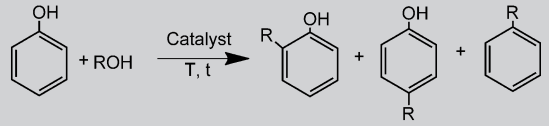

Entry	Substrate	Catalyst	C_{phenol} [%][b]	$Y_{alkylphenol}$ [%][c]	*o*/*p*[d]	Y_{ether} [%][e]	S_{alkyl} [%][f]
1	ethanol	Mgβ(50)[g]	62.7	41.0	63/37	16.4	91.5
2		$Cr_{r(ex)}$-Mgβ[h]	69.7	42.2	60/40	16.9	84.8
3	2-propanol	Mgβ(50)[i]	82.7	65.2	77/23	6.0	86.1
4		$Cr_{(ex)}$-Mgβ[h]	81.5	62.6	68/32	5.1	83.1
5	*tert*-butanol	Mgβ(50)[j]	63.9	25.1	5/95	18.7	68.5
6		$Cr_{(ex)}$-Mgβ[h]	65.8	26.0	5/95	19.5	69.1

[a] Reaction conditions: 10 mmol phenol, 35 mmol alcohol, 0.1 g catalyst. [b] Conversion: [mmol (phenol converted)]/[mmol (phenol initial)]×100. [c] Yield: [mmol (alkylphenols)/[mmol (phenol initial)]×100. [d] The molar ratio of *o*- to *p*-product. [e] Yield: [mmol (aromatic alkyl ether)]/[mmol (initial phenol)]×100. [f] Selectivity of the alkylation product: [mmol (alkylphenols+ether)]/[mmol (initial phenol)]×100. [g] 185 °C, 18.5 h. [h] 205 °C, 18 h. [i] 195 °C, 18 h. [j] 200 °C, 18.5 h.

$Cr_{(ex)}$-Mgβ higher than or comparable to that over Mgβ(50). Further, the product distribution for ethanol and isopropanol is same as that for methanol, suggesting that they follow a similar catalytic route as that in Scheme 1 A. Amazingly, excellent stereo- and regioselectivity (95 % for *p*-product) is detected for *tert*-butyl alcohol. This arises from the special nano-confinement of the limited zeolitic micropores: the 12-MR channels of the BEA zeolite mostly hinder attack at *o*-position towards the bulkier product *o*-*tert*-butylphenol, as reflected by Scheme 1 B. Zeolites as solid acids have exhibited shape-selectivity in many acid reactions,[55,56] but this shape-selective behavior is scarcely found in base or acid–base reactions. For the first time, we observe an acid–base synergetic shape-selective catalysis with the Mg-bearing BEA zeolite.

Conclusions

Mgβ zeolites possessing both superior acidity and basicity were hydrothermally synthesized, which results in their use in the highly efficient alkylation of phenol with alcohols under the desirable low-temperature liquid-phase conditions. The unexpectedly high activity comes from the synergetic effect of adjacent acid–base pairs on the BEA zeolite framework. Stable recyclability with higher activity is achieved by modifying Mgβ with Cr ion-exchange. Alkylation of phenol with different alcohols is also achieved on these Mg-bearing zeolites. Remarkable stereo- and regioselectivity is obtained on a bulky substrate, rendering an efficient shape-selective catalysis.

Experimental Section

Materials and methods

Magnesium (Mg)-bearing BEA zeolites (Mgβ) were synthesized through an acidic co-hydrolysis route. The process was performed as follows. The mixed solution of magnesium nitrate hexahydrate ($Mg(NO_3)_2{\cdot}6H_2O$, 99 wt %, Sinopharm Chem. Reagent Co., AR) and tetraethylorthosilicate (TEOS, 28.4 wt % SiO_2, Sinopharm Chem. Reagent Co., AR) was hydrolyzed under moderately acidic conditions (pH≈0.6) by adding concentrated hydrochloric acidic (HCl, 36.5 wt %, Shanghai Chem. Reagent Co., AR) dropwise at 90 °C within 4 h. Then, tetraethylammonium hydroxide (TEAOH, 35 wt % aqueous solution, Jintan Huadong Chem. Res. Institute, AR) and sodium aluminate ($NaAlO_2$, 41 wt % Al_2O_3, Shanghai Chem. Reagent Co., AR) were added into the above mixture one by one. The obtained slurry was aged at room temperature for 24 h. The final molar composition of the gel was 1 SiO_2/ 0.025 Al_2O_3/ 0.02 MgO/ 0.35 TEAOH/ 22.5 H_2O with the pH value of 12.5. Finally, the resulting gel was transferred into a Teflon-lined stainless steel autoclave and heated statically at 140 °C for 14 d. The products were separated by centrifugation, washed with deionized water, and dried at 100 °C for 12 h. After that, they were calcined at 550 °C for 5 h in air. The obtained Mgβ zeolites were denoted as Mgβ(*n*) (*n*=Mg/Si molar ratio in the synthesis gel).

Characterization

X-ray diffraction (XRD) patterns were characterized with a Smart Lab diffract meter (Rigaku) equipped with a 9 kW rotating anode Cu source (45 kV, 100 mA, 5–50°, 0.2° s^{-1}). Morphologies were investigated with a field-emission scanning electron microscope (FE-SEM) instrument (HITACHI S-4800). Transmission electron microscopy and corresponding elemental mapping images were taken with a JEM-2100F electron microscope with an acceleration voltage of 200 kV. Nitrogen sorption experiments were used to detect the porosity. The isotherms were measured at 77 K (the temperature of liquid nitrogen) with a BELSORP-MINI analyzer. Before analysis, the samples were degassed at 300 °C for 3 h. Fourier transform infrared (FTIR) spectra from 4000 to 400 cm^{-1} were recorded with an Agilent Cary 660 instrument by using KBr disks. Solid-state UV/Vis spectra were recorded with a SHIMADZU UV-2600 spectrometer with barium sulfate ($BaSO_4$) as the internal standard. Inorganic chemical compositions were analyzed with a Jarrell-Ash 1100 in-

ductively coupling plasma (ICP) spectrometer. The surface chemical composition was analyzed by X-ray photoelectron spectra (XPS) with a PHI 5000 Versa Probe X-ray photoelectron spectrometer equipped with AlK_α radiation (1486.6 eV). ^{29}Si and ^{27}Al magic-angle spinning (MAS) nuclear magnetic resonance (NMR) spectra were recorded with a Bruker AVANCE III 600 spectrometer. Thermogravimetric (TG) curves were determined by using a STA409 instrument in dry air at a heating rate of 10 °C min^{-1}. Ammonia (NH_3) and carbon dioxide (CO_2) temperature-programmed desorption (TPD) curves were detected by using a Catalyst Analyzer BELCAT-B. Samples were pretreated at 550 °C for 2 h, and then cooled to 50 °C under helium (He) gas. Adsorption of NH_3 or CO_2 was carried out at 50 °C for 30 min under NH_3/He or CO_2. After the samples were purged under He gas for 30 min, the temperature was increased to 700 °C (8 °C min^{-1}). The desorbed gas was determined by using a Gow-Mac thermal conductivity detector (TCD). In situ FTIR spectra were recorded with an Agilent Cary 660 spectrometer with a mercury cadmium telluride (MCT) detector at a resolution of 4 cm^{-1}. The samples were placed in a Harrick Scientific-made DRIFTS cell with a ZnSe window (Model WMD-U23) and in situ heated to 823 K for 5 h at a heating rate of 10 K min^{-1} in 99.99% pure N_2 stream (8 mL min^{-1}). The sample was then cooled to 463 K and 200 μL of the target compound was introduced separately for 10 min in the N_2 flow. The spectra were collected at 1, 5, 10, 20, and 30 min after the introduction of adsorbents until the spectra remained unchanged. Only the unchanged spectrum collected in the last scan is presented to avoid repetition.

Catalysis tests

The alkylation of phenol was carried out in a 10 mL high-pressure reactor. In a typical run, phenol (10 mmol) and alcohol (35 mmol) were mixed, followed by the addition of the catalyst (0.1 g). The reactor was heated to 190 °C for 18 h with stirring. After the reaction, 1,4-dioxane (0.05 g) was added as an internal standard. The solid was separated by centrifugation and the liquid was analyzed by gas chromatography (Agilent GC 7890B) equipped with a flame ionization detector (FID) detector and a capillary column (HP-5; 30 m × 0.32 mm × 0.25 m). The identification of the products was performed by GC-MS (Agilent 7920A/5975). The major byproduct was aromatic alkyl ethers; each of the others, such as methylanisole (2-methylanisole, 3-methylanisole), dimethylphenol (2,6-dimethylphenol, 2,3-dimethylphenol, 3,4-dimethylphenol), trimethylphenol (2,3,6-trimethylphenol, 2,3,5-trimethylphenol, 3,4,5-trimethylphenol), tetra-methylated phenols and penta-methylated phenols, were found in trace amounts only (yield < 0.5%).

The reusability was assessed in a recycling test. After the reaction, the catalyst was separated by filtration, washed, dried, and calcined at 550 °C for 5 h. The recovered catalyst was then charged into the next run for reuse.

Acknowledgments

The authors thank the National Natural Science Foundation of China (Nos. 21136005, 21303084, and 21476109), Jiangsu Provincial Science Foundation for Youths (No. BK20130921), Specialized Research Fund for the Doctoral Program of Higher Education (No. 20133221120002) and PAPD.

Keywords: alkylation of phenols · bifunctional heterogeneous catalysis · green chemistry · shape selectivity · zeolites

[1] W. Kim, J.-C. Kim, J. Kim, Y. Seo, R. Ryoo, *ACS Catal.* **2013**, *3*, 192–195.
[2] G. Cahiez, V. Habiak, C. Duplais, A. Moyeux, *Angew. Chem. Int. Ed.* **2007**, *46*, 4364–4366; *Angew. Chem.* **2007**, *119*, 4442–4444.
[3] J. Shi, Y. D. Wang, W. M. Yang, Y. Tang, Z. K. Xie, *Chem. Soc. Rev.* **2015**, *44*, 8877–8903.
[4] A. Alotaibi, H. Bayahia, E. F. Kozhevnikova, I. V. Kozhevnikov, *ACS Catal.* **2015**, *5*, 5512–5518.
[5] J. H. Ahn, R. Kolvenbach, C. Neudeck, S. S. Al-Khattaf, A. Jentys, J. A. Lercher, *J. Catal.* **2014**, *311*, 271–280.
[6] H. E. van der Bij, B. M. Weckhuysen, *Chem. Soc. Rev.* **2015**, *44*, 7406–7428.
[7] C. N. Dai, Z. G. Lei, J. Zhang, Y. X. Li, B. H. Chen, *Chem. Eng. Sci.* **2013**, *100*, 342–351.
[8] D. B. Lukyanov, T. Vazhnova, *J. Catal.* **2008**, *257*, 382–389.
[9] T. De Baerdemaeker, B. Yilmaz, U. Muller, D. D. Vos, *J. Catal.* **2013**, *308*, 73–81.
[10] T. Vazhnova, S. P. Rigby, D. B. Lukyanov, *J. Catal.* **2013**, *301*, 125–133.
[11] J. L. Hodala, Y. S. Bhat, A. B. Halgeri, G. V. Shanbhag, *Chem. Eng. Sci.* **2015**, *138*, 396–402.
[12] G. Y. Jeong, A. K. Singh, S. Sharma, K. W. Gyak, R. A. Maurya, D. P. Kim, *NPG Asia Mater.* **2015**, *7*, e173–e180.
[13] G. Wong-Parodi, T. Krishnamurti, A. Davis, D. Schwartz, B. Fischhoff, *Nat. Clim. Change* **2016**, *6*, 563–569.
[14] J. N. Chheda, G. W. Huber, J. A. Dumesic, *Angew. Chem. Int. Ed.* **2007**, *46*, 7164–7183; *Angew. Chem.* **2007**, *119*, 7298–7318.
[15] D. S. Sholl, R. P. Lively, *Nature* **2016**, *532*, 435–437.
[16] J. Li, X. C. Wang, G. J. Chen, D. F. Li, Y. Zhou, X. N. Yang, J. Wang, *Appl. Catal. B* **2015**, *176*, 718–730.
[17] Q. Wang, X. C. Cai, Y. Q. Liu, J. Y. Xie, Y. Zhou, J. Wang, *Appl. Catal. B* **2016**, *189*, 242–251.
[18] K. F. Liu, S. J. Xie, S. L. Liu, G. L. Xu, N. N. Gao, L. Y. Xu, *J. Catal.* **2011**, *283*, 68–74.
[19] Z. W. Qi, R. S. Zhang, *Ind. Eng. Chem. Res.* **2004**, *43*, 4105–4111.
[20] A. R. Gandhe, J. B. Fernandes, *Catal. Commun.* **2004**, *5*, 89–94.
[21] R. Bal, S. Sivasanker, *Appl. Catal. A* **2003**, *246*, 373–382.
[22] F. Cavani, L. Maselli, S. Passeri, J. A. Lercher, *J. Catal.* **2010**, *269*, 340–350.
[23] M. Bregolatoa, V. Bolis, C. Busco, P. Ugliengo, S. Bordiga, F. Cavani, N. Ballarini, L. Maselli, I. Rossetti, L. Forni, *J. Catal.* **2007**, *245*, 285–300.
[24] M. E. Sad, C. L. Padro, C. R. Apesteguıa, *Appl. Catal. A* **2008**, *342*, 40–48.
[25] S. Barman, N. C. Pradhan, J. K. Basu, *Catal. Lett.* **2006**, *111*, 67–73.
[26] M. C. Samolada, E. Grigoriadou, Z. Kiparissides, *J. Catal.* **1995**, *152*, 52–62.
[27] Y. L. Wang, Y. Y. Song, W. X. Zhang, *Chem. Eng. J.* **2012**, *181–182*, 630–635.
[28] P. Łysik, A. Górska, S. Szarlik, *Ind. Eng. Chem. Res.* **2014**, *53*, 17558–17562.
[29] R. Klimkiewicz, H. Grabowska, W. Mista, K. Przybylski, *Ind. Eng. Chem. Res.* **2012**, *51*, 2205–2213.
[30] V. Crocellà, G. Cerrato, G. Magnacca, C. Morterra, F. Cavani, L. Maselli, S. Passeri, *Dalton Trans.* **2010**, *39*, 8527–8537.
[31] S. Velu, C. S. Swamy, *Appl. Catal. A* **1994**, *119*, 241–252.
[32] C. T. O'Connor, S. Sauerbeck, G. Moon, W. Böhringer, J. C. Q. Fletcher, From Zeolites to Porous MOF Materials—The 40th Anniversary of the International Zeolite Conference **2007**, 1088–1095.
[33] L. F. González Peña, M. E. Sad, C. L. Padró, C. R. Apesteguía, *Catal. Lett.* **2011**, *141*, 939–947.
[34] G. Moon, W. Bohringer, C. T. O'Connor, *Catal. Today* **2004**, *97*, 291–295.
[35] C. Wang, A. Q. Wang, J. Xu, N. D. Feng, F. Deng, *Angew. Chem. Int. Ed.* **2016**, *55*, 2507–2511; *Angew. Chem.* **2016**, *128*, 2553–2557.
[36] A. Primo, H. Garcia, *Chem. Soc. Rev.* **2014**, *43*, 7548–7561.
[37] H. Awala, J. P. Gilson, R. Retoux, P. Boullay, J. M. Goupil, V. Valtchev, S. Mintova, *Nat. Mater.* **2015**, *14*, 447–451.
[38] T. W. Kim, S. Y. Kim, J. C. Kim, Y. J. Kim, R. Ryoo, C. U. Kim, *Appl. Catal. B* **2016**, *185*, 100–109.

[39] A. Mekki-Berrada, S. Bennici, J. P. Gillet, J. L. Couturier, J. L. Dubois, A. Auroux, *J. Catal.* **2013**, *306*, 30 – 37.
[40] J. D. Lewis, S. V. D. Vyver, Y. R. Leshkov, *Angew. Chem. Int. Ed.* **2015**, *54*, 9835 – 9838; *Angew. Chem.* **2015**, *127*, 9973 – 9976.
[41] M. J. Climent, A. Corma, H. Garcia, R. Guil-Lopez, S. Iborra, V. Fornes, *J. Catal.* **2001**, *197*, 385 – 393.
[42] Y. J. Wu, J. Wang, P. Liu, W. Zhang, X. J. Wang, *J. Am. Chem. Soc.* **2010**, *132*, 17989 – 17991.
[43] J. Gu, Y. H. Jin, Y. Zhou, M. J. Zhang, Y. J. Wu, J. Wang, *J. Mater. Chem. A* **2013**, *1*, 2453 – 2460.
[44] B. O. Hincapie, L. J. Garces, Q. Zhang, A. Sacco, S. L. Suib, *Microporous Mesoporous Mater.* **2004**, *67*, 19 – 26.
[45] Y. Zhou, Y. H. Jin, M. Wang, W. Zhang, J. Y. Xie, J. Wang, L. M. Peng, *Chem. Eur. J.* **2015**, *21*, 15412 – 15420.
[46] C. D. Wanger, W. M. Riggs, L. E. Davis, J. F. Muilenberg, *Handbook of X-ray Photoelectron Spectroscopy*, PerkinElmer, Eden Prairie, MN, **1979**.
[47] T. L. Barr, M. A. Lishka, *J. Am. Chem. Soc.* **1986**, *108*, 3178 – 3186.
[48] M. Huang, A. Adnot, S. Kaliaguine, *J. Am. Chem. Soc.* **1992**, *114*, 10005 – 10010.
[49] J. Y. Xie, H. M. Wen, W. Zhang, Y. Zhou, J. Wang, *CrystEngComm* **2016**, *18*, 1164 – 1173.
[50] M. D. S. Machado, J. Perez-Pariente, E. Sastre, D. Cardoso, M. V. Giotto, J. L. Garcia-Fierro, V. Fornes, *J. Catal.* **2002**, *205*, 299 – 308.
[51] F. Frusteri, M. Cordaro, C. Cannilla, G. Bonura, *Appl. Catal. B* **2015**, *162*, 57 – 65.
[52] S. Sato, K. Koizumi, F. Nozaki, *J. Catal.* **1998**, *178*, 264 – 274.
[53] T. Mathew, M. Vijayaraj, S. Pai, B. B. Tope, S. G. Hegde, B. S. Rao, C. S. Gopinath, *J. Catal.* **2004**, *227*, 175 – 185.
[54] C. E. Hetrick, J. Lichtenberger, M. D. Amiridis, *Appl. Catal. B* **2008**, *77*, 255 – 263.
[55] B. Smit, T. L. M. Maesen, *Nature* **2008**, *451*, 671 – 678.
[56] M. Dusselier, P. V. Wouwe, A. Dewaele, P. A. Jacobs, B. F. Sels, *Science* **2015**, *349*, 78 – 80.

Manuscript received: September 9, 2016

Final Article published: ■■ ▮▮, 0000

Acid–base synergetic sites with enhanced basicity without compromising acidity are constructed on the Mg-bearing BEA zeolite by incorporating Mg ions into the framework in a direct synthesis route. As a result, the Mg-bearing zeolite triggers the first efficient low-temperature liquid-phase alkylation of phenol with high yield, stable reusability, good substrate compatibility, and unique shape selectivity.

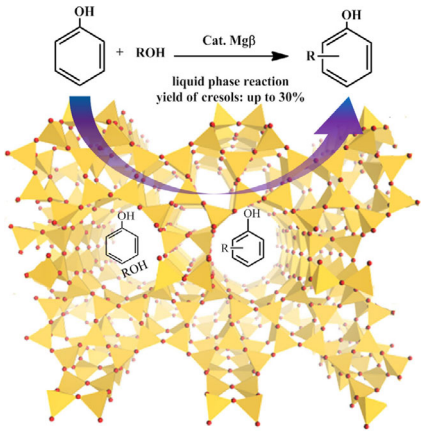

J. Xie, W. Zhuang, W. Zhang, N. Yan, Y. Zhou, J. Wang**

■■ – ■■

Construction of Acid–Base Synergetic Sites on Mg-bearing BEA Zeolites Triggers the Unexpected Low-Temperature Alkylation of Phenol